Vietnam Journal of Catalysis and Adsorption
Tạp chí xúc tác và hấp phụ Việt Nam

https://chemeng.hust.edu.vn/jca/

Highly efficient adsorption of dye using novel reduced graphene oxide/halloysite nanocomposite

Ngo Ha Son *, Nguyen Thi Linh

Department of Oil Refining and Petrochemistry, Hanoi University of Mining and Geology
**Email: ngohason@humg.edu.vn*

ARTICLE INFO

Received: 15/4/2022
Accepted: 20/5/2022
Published: 20/6/2022

Keywords:

Dye adsorption, reduced graphene oxide, halloysite, nanocomposite, kinetics.

ABSTRACT

The novel composite nanomaterials were synthesized via a simple method from two natural clay mineral sources, graphite and halloysite. The materials were characterized by X-ray diffraction (XRD), scanning electron microscopy (SEM), transmission electron microscopy (TEM), Fourier transform infrared (FTIR), Brunauer-Emmet-Teller (BET) methods. The results showed that halloysite nanotubes are successfully intercalated between the graphene oxide layers. The adsorption capacity of the material with RY-145, a typical dye in textile wastewater, was evaluated. Also, the effects of adsorption time, initial concentration of pollutant, adsorbent dosage, speed of agitation and temperature were investigated. The adsorption efficiency of the material for RY-145 dye is about 99% after 4 hours with the high initial concentration of pollutant of 50ppm. Adsorption kinetics of the material for RY-145 match the pseudo-second order kinetic of Langmuir adsorption model. The outstanding performance of the nanocomposite as an adsorbent highlight the promising applications of the novel material in was water treatment processes.

Introduction

Dyes are chemical compounds that bind to the surface of a fabric to create colour. Most dyes are complex organic molecules that resisting to detergents. Synthetic dyes are widely used in many industrial fields, for example, in the textile industry [1], the paper industry [2] or tanning processes [3], food processing, plastics, cosmetics, rubber, printing and dye manufacturing [4], [5], [6]. Their release into the hydrosphere generates a significant source of pollution because of the persistent property of these organic compounds. This will produce undesirable colours in the water, reduce sunlight penetration and prevent photochemical and biological processes that are important to aquatic organisms [7]. According to updated data, there are over 10,000 known commercial dye types with an annual production of over 7×10^5 tons/year [8]. The total consumption of dyes in the textile and apparel industry worldwide is over 10,000 tons/year and about 100 tons/year of dye was discharged into water flows consequently [9]. Various methods such as adsorption, coagulation, advanced oxidation, and membrane separation are used to remove dyes from wastewater [10]. Adsorption is one of the most efficient processes that industries used to reduce harmful inorganic/organic pollutants present in wastewater [11]. Generally, textile industries use high–cost commercial activated carbon to treat dyeing wastes. Current research is focusing on materials to

https://doi.org/10.51316/jca.2022.040

effectively replace commercial activated carbon. Several scientists have reported the feasibility of using a variety of low-cost adsorbents derived from natural materials, industrial waste, agricultural by-products, and biological adsorbents as pre-eminent substance [12]. Apart from that, researchers have also reported different physical or chemical treatment methods which have been applied to raw biomass adsorbents to improve their adsorption capacity [12].

Graphene, a monolayer of sp^2 hybrid carbon atoms arranged in hexagonal rings, has attracted huge interest by its unique features during the past decade [13], [14], [15], [16]. Graphene oxide (GO) is acquired through oxidation and reduced graphene oxide (rGO) is the main product of reduction process of GOare. Both of which possess carboxylic acid, phenol hydroxyl and epoxide groups but differ in quantity [17], [18], [19]. They are two of the materials capable of eliminating contaminants from waste water [20], [21], [22]. However, the very good dispersion of GO in solvents makes it difficult to separate, while rGO is rarely used as an adsorbent due to its poor dispersion in water. In addition, as an adsorbent, the adhesion of rGO sheets make it have less available room for adsoprtion and consequently decrease its activity. Therefore, many inorganic nanoparticles (NPs) including clay particles were anchored to the graphene-based plane to modify the surface properties [23], [24], [25], [26], [27], [28]. In such nanocomposites, their high surface area and pore volume make them be favourable for removal of contaminants [29], [30], [31]. According to this idea, the intecalation of stable structure between rGO sheets to improve its adsorption capacity is one of the novel and potential solution.

Halloysite nanotube (HNT) is a component of kaolin mineral. Its chemical formula is $Al_2Si_2O_5(OH)_4$. nH_2O with the outer diameter is about 40-60 nm, the inner diameter is 10-15 nm, and the length of the tubes is about 500-1500 nm. Structurally, unlike kaolinite, the halloysite has a layer of water atoms present among layers of aluminium and silica structure. Basically, halloysite has been used to manufacture high-quality ceramics, crucibles, etc. However, recently, due to its superior properties such as catalytic ability thanks to its composition of aluminium and silica, with a large specific surface area, porous structure, non-toxic, mechanical stability, resistance to organic solvents, capability of structure and surface modification, low cost, this material has been applied in many technological processes [32] [33] [34]. One of which is the fabrication of adsorbents for environmental treatment by synthesizing HNTs combined with graphene [35], [36]. HNTs intercalating between graphene sheets can efficiently enhance specific surface area and pore volume. These structural characteristics make the composite ideal for eliminating dyes from aqueous environments. To the best of our knowledge, there is lack of research on kinetic of dye adsorption on such material.

In this paper, the purification process of halloysite from raw halloysite mineral is presented. The nanoscale halloysite tube is then intercalated into the reduced graphene to form a composite material. Adsorption capacity, adsorption kinetics and the influence of the conditions of the adsorption process are also investigated and analysed.

Experimental

Chemicals

Raw graphite was obtained from Lao Cai, Vietnam while and raw halloysite was provided directly from mines in Phu Tho, Vietnam. These raw materials were dried to remove free adsorbed water, then was grinded and purified. Crystalline $KMnO_4$ 98%, H_2O_2 30%, hydrochloric acid, sulfuric acid 98%, Na_2NO_3, hydrazine and RY-145 dye are all purchased from China. The chemicals were used directly without any further purification and treatment.

Synthesis of graphene oxide

Graphene oxide was synthesized from graphite by Hummers method [37]. In a typical experiment, 5 g of graphite powder was added to 42 ml of H_2SO_4 98% at the temperatures below 5°C. The solution was continuously stirred with the speed of 400 rpm for 30 minutes until the solution turned into black. Then, 15 g of $KMnO_4$ was added and the temperature was maintained lower than 20ºC for 4 hours. Next, 140 ml H_2O was slowly inserted, and the temperature was kept below 50°C for 3 hours. In the following step, 50 ml of H_2O_2 30% was gradually poured into the solution under stirring for 20 minutes until it turned into light brown colour. After that, 300 ml of HCl 0.1M solution was added. The bottom residue was separated, filtered, and washed until pH = 7 was reached. The sample underwent ultrasonic vibration for 30 minutes, then was dried at 70°C to finally achieve graphene oxide.

Halloysite purification

https://doi.org/10.51316/jca.2022.040

Halloysite minerals derived from Vietnamese kaolin sources were grinded and sieved to remove impurities. Firstly, 20 g of raw halloysite was taken and dried at 100ºC for 3 hours, then was dispersed in 27.5 ml of distilled water. Then, 1 ml of 98% H_2SO_4 solution was slowly added under stirring at 90°C within 2 hours. The resulting solution was filtered and rinsed several times with distilled water to remove excess H_2SO_4 and was then dried. After that, 750 ml of distilled water was added to the dried sample and the mixture was stirred for 24 hours. The obtained solution was settled for 96 hours, then was filtered and decanted to remove the upper part. The obtained solid was washed with distilled water several times, centrifuged and dried to acquire purified halloysite.

Preparation of HNT/rGOcomposite

HNT/rGO nanomaterials was synthesized in accordance with the following procedure: 100 mg of HNT was dispersed in 50 ml of distilled water with ultrasonic vibration for 10 minutes (solution 1). At the same time, 200 mg of GO was dispersed in 200 ml of distilled water under ultrasonic vibration for 10 minutes (solution 2). Later, solution 1 was combined with solution 2 and the mixture was stirred at 90°C for 10 minutes and underwent ultrasonic vibration for 30 minutes. Then, 2 ml of hydrazine 80% was slowly added and stirring conditions was retained for 2 hours further. The residue was then filtered and dried to obtain HNT/rGOmaterial.

Material characterizations

Scanning electron microscopy (SEM) and transmission electron microscopy (TEM) images were taken to determine the structure on the surface of the material. SEM images of prepared materials were obtained on a JSM-6701F (Jeol). The SEM sample was made by distributing a small amount of suspension on a piece of silicon wafer. TEM images were investigated by TEM-JEOL-2010 200kV apparatus.

X-ray diffraction (XRD) using Cu Kα radiation, λ = 1,5403 with scanning range 2λ = 5-80ºC was recorded by D8-Bruker. The FTIR spectroscopic was carried out to investigate the binding characteristics of the material on the Jasco FT/IR-4600 device.

The UV-VIS spectra with the wavelength range of 200 to 800 nm were recorded on the apparatus Jasco V-750 to identify bandgap energy of materials and quantify the removal of pollutant after the adsorption process.

N_2 adsorption-desorption isotherm method (BET) was performed by Chem BET - 3030 at a temperature of 77.34ºC to determines the specific surface area as well as the pore size distribution of the material. The point of zero charge of the nanocomposite was determined using drift method [38].

Evaluation of the adsorption capacity

To evaluate the adsorption capability of the synthesized HNT/rGO composite, experiments were carried out with the following conditions: the initial concentration of RY-145 in the solution is 50 ppm and material weight is 0.21 g.

The adsorption efficiency is calculated by the formula:

$$H\,(\%) = (C_o - C)/C_o \times 100 \quad (1)$$

In which: Co and C are the concentrations of contaminant at the beginning and after the experiment (mg/L). The concentrations of pollutant in the solution were calculated based on the optical absorbance capacity at the wavelength of 541nm and the calibration curve of already known concentrations that was built previously.

Reusability of the material as adsorbent

The dyeloaded on HNT/rGO were regenerated by desorption reagent which is HCl 0.1M. In a typical treament, 0.21 g of RY 145-loaded material were dispersed in 50 mL HCl 0.1M, and shaken vigorously for 24 h at 293 K. After that, the solid phase was obtained by centrifugation (6000 rpm, 20 mins). Then, the collected material was rinsed with distilled water, dehydrated in an oven at 60ºC for 8 h. The final solid would be used for the next adsorption experiments.

Results and discussion

Material characterization

Figures 1 A, B, C and D illustrates the SEM and TEM results of the composite. The images suggest that halloysite nanotubes were uniformly distributed between the GO layers and tightly attached to those layers. The presence of HNT established rooms between rGO sheets that might increase the isolation of GO layers to form 3D-shaped composite.

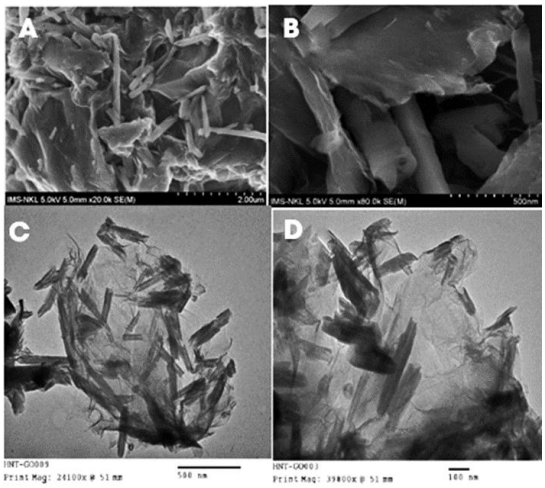

Figure 1: SEM image (a), (b) and TEM (c), (d) image of HNT/rGO material

X-Ray results were recorded in the range of 2θ from 5 to 80º. Findings indicate that the typical peaks of the purified halloysite material appeared at 2θ = 12.20; 19.90; 24.84; 35.02; 37.98; 54,34; 62.5º (Figure 2B) are consistent with the standard halloysite X-ray diffractions obtained in other publications [39] [40] . X-ray results of GO (Figure 2A) do not show any diffraction peak of graphite at 2θ = 26.5º but a peak at 2θ = 11.12º emerged. This means that groups containing oxygen such as hydroxyl (-OH), epoxy (-O-), carbonyl (-C = O), carboxylic (-COOH), etc., were formed and inserted into the space between layers of graphite resulted in the upsurge of the space between layers. indicates The only one strong peak at 2θ = 11.12º of GO representing for high purity level. The distinctive reflection peaks of halloysite appear in all X-ray spectra of HNT/rGO material samples (Figure 2c) but the typical peak of GO was not clearly visible. This could be explained by the coverage of HNT over the typical peak of GO peak at the same reflection angle.

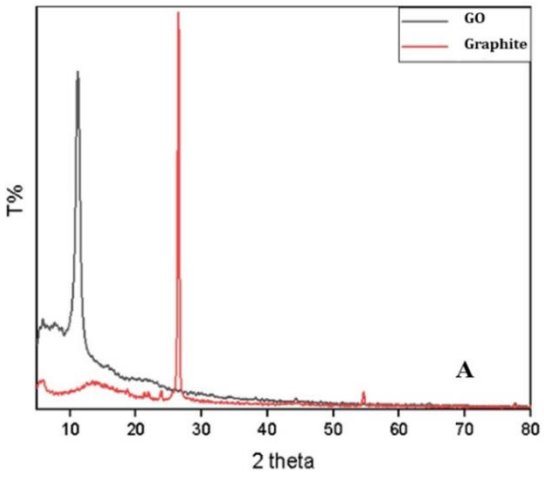

Figure 2A: XRD spectrum of GO and graphite

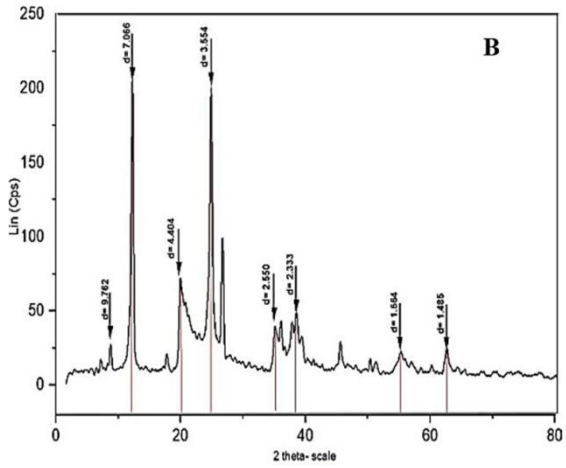

Figure 2B: XRD spectrum of HNT

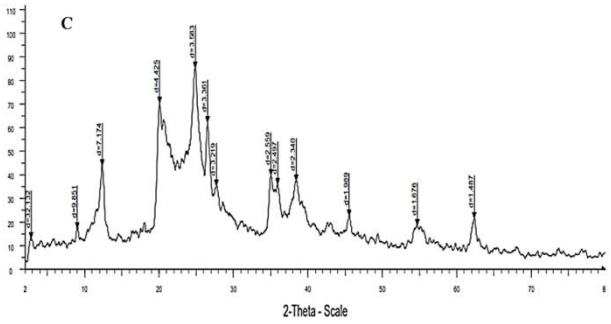

Figure 2C: XRD spetrum of HNT/rGO

To clarify the structural features of the material, the results of the FTIR infrared spectroscopy of the material were shown in Figure 3.

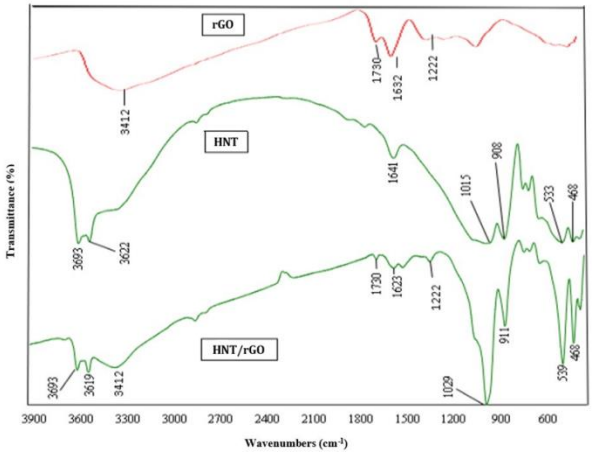

Figure 3: FTIR spectrum of GO, HNT and HNT/rGO material

For GO sample, the wavelengths at 3426 cm^{-1} signify for OH group. Besides, the main functional groups containing oxygen (C - O and C = O) are found at the oscillations of 1100 cm^{-1} and 1730 cm^{-1} while other functional groups such as C = O and C = C could be assigned to the peak at 1225 cm^{-1} at 1617 cm^{-1},

respectively. The peaks recorded with purified HNT material sample at 3622 cm^{-1} and 3693 cm^{-1} characterized for O-H bond of Si-OH silanol group and OH group of the water molecule on the material surface. The peak at wavelength of 1641 cm^{-1} corresponds to the H-OH bond of water in halloysite molecule. In addition, the peak at 1115 cm^{-1} indicates the existence of the Si-O-Si group in the center of the tetrahedron and the peak at 1109 cm^{-1} stands for the link of Si-O group. The O-H group of the internal Al-OH is characterized by a peak of 906 cm^{-1} while the peak at wavelength of 533 cm^{-1} is attributed to the Si-O bond. HNT/rGO composites have all the above typical peaks. Specifically, the peak at 3412 cm^{-1} is a prolonged oscillation in the hydroxyl group of GO and HNT. The oscillations at 1029 cm^{-1} are ascribed to the tetrahedral Si-O-Si group. The characteristic oscillation at a wavelength of 911 cm^{-1} signifies the O-H bond of the Al-OH group inside the material. The 1370 cm^{-1} peak corresponds to the C-O bond of GO whereas the peak at 1623 and 1222 cm^{-1} corresponds to the C = C and C-O bond of the aromatic ring.

The specific surface area of the material is determined by Nitrogen adsorption - desorption at 77.3K isotherm (Figure 4). The results revealed that the N_2 adsorption isotherm of TiO_2-HNT/GO at 77.3K has the hysteresis of IV type which is in compliance to the IUPAC classification of mesoporous material.

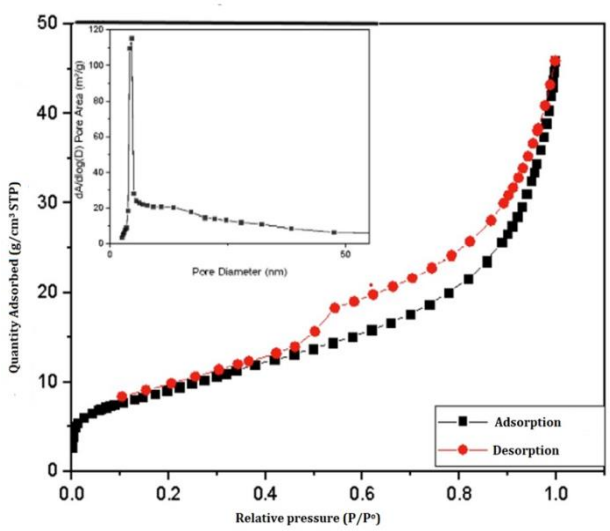

Figure 4: N_2 adsorption-desorption isothermal curve and pore size distribution of HNT/rGO

The specific surface area of the material was assessed to be 51.4 m^2/g, which is attributed to be the surface area of the halloysite since rGO is difficult to measure surface area using the conventional BET method when they are linked with halloysite. However, this measured area was higher than that of a single halloysite nanotube (approximately 40 m^2/g). Besides, the average pore diameter of the obtained composites is about 8.4 nm. Such mesopore size is well-suited for adsorption and catalysis applications.

With a relatively large surface area and suitable pore size, it facilitates the adsorption of pollutants onto the porous system, contributing to enhance the adsorption efficiency of the material.

Evaluation of adsorption capacity

Experiments were carried out to evaluate the adsorption capacity of RY-145 dyes at room temperature, with an initial concentration of RY-145 of 50 ppm. Three samples were used in the process for comparison: rGO, HNT, HNT/rGOand the achieved results are given in figure 5.

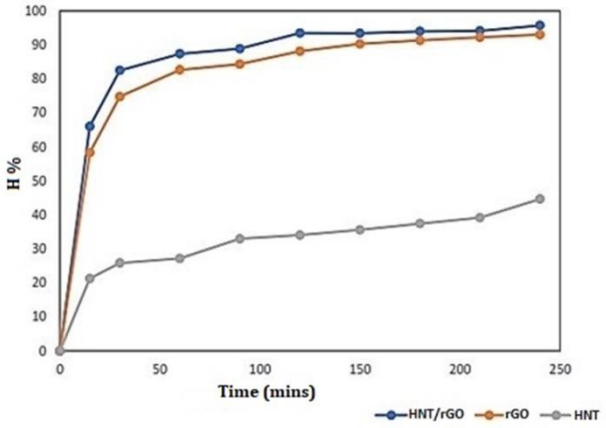

Figure 5: Adsorption efficiency of GO, HNT, HNT/rGO

Figure 5 points out that the adsorption efficiency after 240 mins of HNT/rGO is 98%, that of HNT is 45% and that of rGO is 93%. This is a proof that HNT/rGO has better adsorption capacity than pure rGO and pure HNT because anchoring HNT into GO expands the space between the GO layers, thereby generating more adsorption space and boosting adsorption efficiency accordingly. Also, it can be concluded that the adsorption performance of the nanocomposite might arise from the physical adsorption on the surface of rGO. The strong hydrophobic interactions (π–π stacking) could be formed between the hydrophobic basic surface of the rGO nanosheets and the aromatic rings in RY-145 structure. This phenomenon is primarily responsible for the outstanding adsorption of composite and rGO. Considering the role of HNT, although the gibbsite octahedral sheet (Al-OH) groups on the internal surface and siloxane groups (Si-O-Si) could help HNTs absorb some reactive dyes by the

hydrogen bonding but it is hard to reach high efficiency. Comparable result was obtained by Liu et al. [41] in the process of RhB treatment.

Also, the pH_{pzc} (point of zero charge) value of the HNT/rGO was also measured using the drift method mentioned above. The pH_{pzc} value for HNT/rGO of about 8.0 was recorded. Theoretically, at pH < pH_{pzc}, the surface of the adsorbent will be in positive charge state while the converse result happens at pH > pH_{pzc}. In our experiment, the pH of the solution was 6.5 and such value created the positive charge for adsorbent surface. Accordingly, this condition favors the adsorption of anionic compound on HNT/rGO surface. RY – 145 is a typical anionic dye and therefore easily adsorbed by HNT/rGO in this case. This explains the excellent efficiency of dye removal at neutral pH of as-prepared HNT/rGO composite. Such conditions would also be more eco-friendly for the dye adsorption processes.

From those, it can be considered that the synthesized nanocomposite could be very effective for anionic dye treatment in aqueous phase.

Effect of adsorbent dosage

The experiments studying the effects of HNT/rGO dosage were conducted with three quantities of 0.15, 0.18, and 0.21 g of rGO/HNT. The ambient temperature was appplied with the contaminant concentration of 50 ppm throughout the period of 240 minutes. Results are shown in the Figure 6.

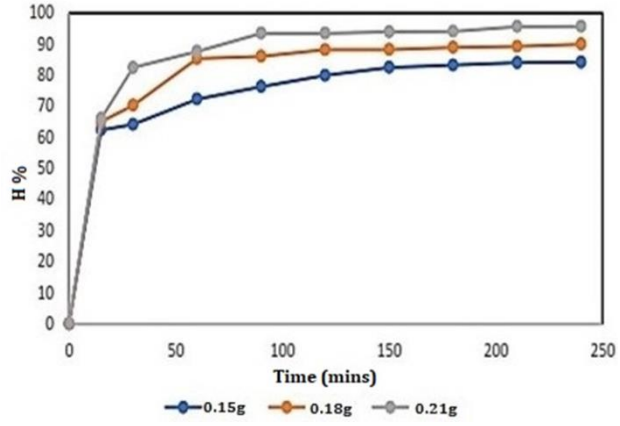

Figure 6: Effect of HNT/rGO dosage on the efficiency of the adsorption process

As illustrated in Figure 6, the material weight has a direct impact on the adsorption capacity. At the loading of 0.15 g, the efficiency attained 84%, when the weight increased to 0.18 and 0.21 g, the adsorption efficiency reached 90% and 98%. Theoretically, the specific surface area, and the number of adsorption centers of the material does not change with a certain material dosage. Therefore, when the loading of adsorbent is small, the adsorption centers will be seized rapidly by the pollutant reducing the free adsorption center at the surface of the material. On the other hand, when the adsorbent used was higher, there are more room for contaminant adsorbed. As a result, the higher loading of adsorbent will increase the adsorption efficiency. The findings are in accordance with published researches [42], [43], [44].

The results also revealed that dye could be completely removed by applying a small amount of material. This prove the potential of prepared composite in waste water treatment applications.

Effects of stirring speed

The effect of stirring speed from 60 to 600 rpm was also investigated, and the obtained results are outlined in the Figure 7.

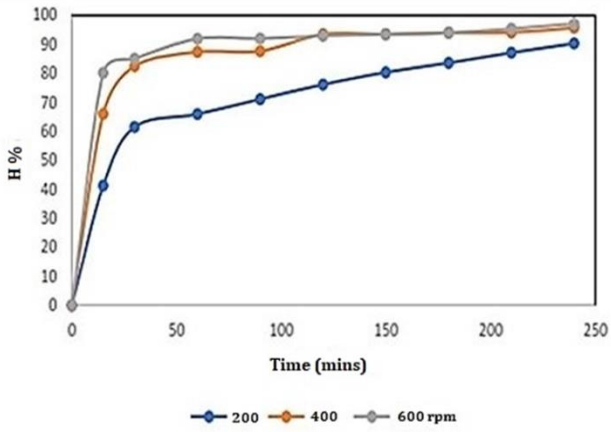

Figure 7: Effect of stirring speed on the adsorption capacity of the material

The stirring speed has a significant impact on the adsorption capacity of the material. When the stirring speed rises, the adsorption efficiency also increases. Specifically, after 90 minutes with a stirring speed of 60 rpm, the adsorption efficiency is only 70%, while with the speed of 400, 600 rpm, the efficiency increases to 87% and 92% respectively. This shows that when increasing the stirring speed, the diffusion ability of the material increases leads to the rise of the contact ability of the material with organic molecules, thereby enhancing the adsorption efficiency of the material. Nevertheless, the utilization of stirring to improve the efficiency of heat transfer and mass transfer in adsorption process of dye but it will consume considerable energy. This conventional results could be

seen in previous publications [45], [46]. However, the mixing efficiency is highly dependent on the viscosity of response system. Therefore, at laboratory scale, stirring speed between 400 rpm and 600 rpm can be chosen to accomplish the maximum adsorption efficiency.

Effect of temperature

Temperature is one of the most crucial factors that has a substantial impact on the adsorption process. To investigate the effect of temperature, the adsorption experiment was performed at three different temperatures: 10ºC, 30ºC and 60ºC with the initial concentration of pollutant is 50 ppm. The results are presented in figure 8.

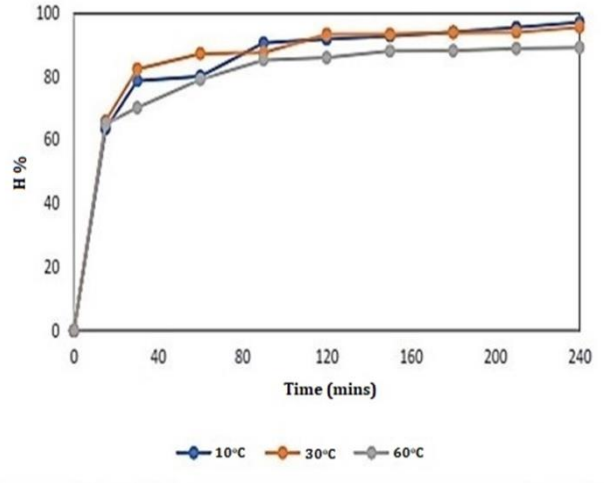

Figure 8: Effect of temperature on the adsorption capacity of the material.

The results demonstrated that if the temperature varies in the range of 10 to 30ºC, there is no effect on the adsorption capacity. as it all reaches saturated adsorption of more than 90% after about 120 minutes. However, when the temperature rises to 60ºC, the adsorption capacity of the material declines to 80%. This can be explained because when the temperature is high, the interaction between molecules of organic compounds and materials decreases that facilitates the desorption trend, so the adsorption efficiency is lower under the same inquiry conditions. Results of the temperature effect on the material's adsorption capacity also show that the material has high adsorption capacity at ambient temperature. This result was also recorded in the past work [47] [48] and is in line with the theory of the general adsorption process. Interestingly, the obtained results are different from results of Çiçek [43] and Ahmad [42] who saw that the adsoprtion capacity increase with temperature. In our case, the ability to efficiently work at ambient temperature could be the important advantage of rGO/HNT

Adsorption kinetics of the material

The adsorption capacity of the material is calculated as follows:

$$q = \frac{(c_o - c)V}{m} \quad (2)$$

C_o and C are the initial concentration and concentration at time t of the adsorbent (mg/l).

V is the volume of solution (l).

M is the mass of the adsorbent (g)

Apparent kinetic equation of first-order model:

$$\frac{dq_t}{d_t} = k_1(q_e - q_t) \quad (3)$$

Apparent kinetic equation of second-order model:

$$\frac{dq_t}{d_t} = k_2(q_e - q_t)^2 \quad (4)$$

In which: k_1, k_2 are reaction rate constants according to kinetic models of first and second-order reactions. q_e, q_t is the adsorption capacity at equilibrium period and time t (mg/g)

The adsorption of the material at different adsorbate concentrations (25, 50, 75 ppm) with an adsorbent weight of 210 mg in 240 minutes was investigated and results are exhibited in Figure 9.

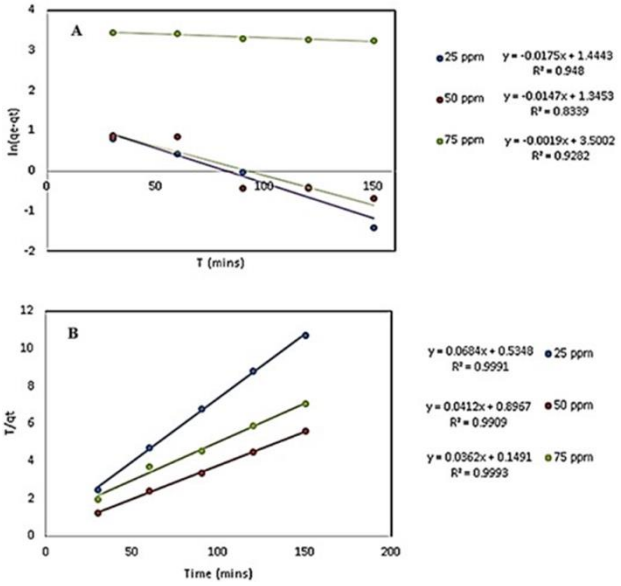

Figure 9: Adsorption kinetics of (A) 1st order; (B) 2nd order model

The chart in Figure 9 is formed based on the relationship between the adsorption time and the

adsorption capacity of the material at different initial contaminant concentrations. From that point, the appropriateness of the adsorption model is based on the calculation of the coefficient R^2.

From the charts shown in Figures 9A, 9B, it can be seen that the first-order kinetic equation has an unreliable linear regression of 0.83 - 0.95 while the second-degree kinetic equation has R from 0.9909 to 0.9993. The calculated q_e value of the second order adsorption kinetic equation is very close to the experiment. Thus, the second order kinetic equation is suitable for explaining the adsorption process.

Reusability of the adsorbent

The reusability of HNT/GO is illustred in Fig. 10. After five adsorption/desorption cycles, the adsorption efficiency of the recycled HNT/GO were still more than 90% with the initial pollutant's concentration of 50ppm. These results suggest that our nanocomposite offered excellent performance after regeneration and economical cost-effective solution benefiting for large-scale purposes.

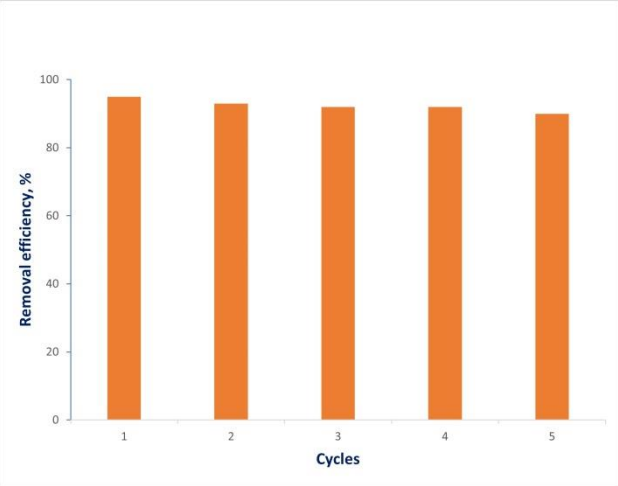

Figure 10: Reusabiltiy of the material in adsorption process

Conclusion

In this study, composite nanomaterials were successfully synthesized from graphite and halloysite sources via simple procedure.The adsorption efficiency of the material for RY-145 dye is 99% after 4 hours, with an initial contaminant concentration of 50 ppm. This number is considerably higher than using only halloysite nanotube or graphene oxide as adsorbent. The adsorption capacity of the material improves with increasing stirring speed and is kept at ambient temperature. Research on adsorption kinetics of the material for RY-145 shows that the adsorption capacity of the material is consistent with the second order adsorption kinetic equation. The highest adsorption content is about 233 mg/g at ambient temperature. In addition, the material shows high perfomance in reusability represented by intact excellent removal efficiency (> 90%) after 5 rounds of recyclabiltiy. The results obtained confirm the high adsorption capacity of the material to the pollutant textile waste and its potential in wastewater treatment process.

Acknowledgments

This research is funded by Vietnam Ministry of Education under grant number B2021 – MDA -02.

References

1. J. Sokolowska-Gajda, H.S. Freeman, A. Reife, Dyes Pigments. 30 (1996) 1–20. https://doi.org/10.1016/0143-7208(95)00048-8.
2. K. Ivanov, Pap. 50 (1996) 456.
3. I. Kabdaşli, O. Tünay, D. Orhon, , Water Sci. Technol. 40 (1999) 261–267. https://doi.org/10.1016/S0273-1223(99)00393-5.
4. N. Bensalah, M.A.Q. Alfaro, C.A. Martínez-Huitle, , Chem. Eng. J. 149 (2009) 348–352. https://doi.org/10.1016/j.cej.2008.11.031.
5. D. Wróbel, A. Boguta, R.M. Ion, J. Photochem. Photobiol. Chem. 138 (2001) 7–22. https://doi.org/10.1016/S1010-6030(00)00377-4.
6. S. Dawood, T.K. Sen, C. Phan, Water. Air. Soil Pollut. 225 (2013) 1818. https://doi.org/10.1007/s11270-013-1818-4.
7. Y.C. Wong, Y.S. Szeto, W.H. Cheung, G. McKay, Process Biochem. 39 (2004) 695–704. https://doi.org/10.1016/S0032-9592(03)00152-3.
8. T.K. Sen, S. Afroze, H.M. Ang, Equilibrium, Water. Air. Soil Pollut. 218 (2011) 499–515. https://doi.org/10.1007/s11270-010-0663-y.
9. M.T. Yagub, T.K. Sen, H.M. Ang, Water. Air. Soil Pollut. 223 (2012) 5267–5282. https://doi.org/10.1007/s11270-012-1277-3.
10. V.K. Gupta, Suhas, , J. Environ. Manage. 90 (2009) 2313–2342. https://doi.org/10.1016/j.jenvman.2008.11.017.
11. R. Kant, , J. Water Resour. Prot. 4 (2012) 93–98. https://doi.org/10.4236/jwarp.2012.42011.
12. M.S.U. Rehman, I. Kim, J.-I. Han, Carbohydr. Polym. 90 (2012) 1314–1322. https://doi.org/10.1016/j.carbpol.2012.06.078.
13. K.S. Novoselov, A.K. Geim, S.V. Morozov, D. Jiang, Y. Zhang, S.V. Dubonos, I.V. Grigorieva, A.A. Firsov, Science. 306 (2004) 666–669. https://doi.org/10.1126/science.1102896.

14. R.R. Nair, P. Blake, A.N. Grigorenko, K.S. Novoselov, T.J. Booth, T. Stauber, N.M.R. Peres, A.K. Geim, Science. 320 (2008) 1308–1308. https://doi.org/10.1126/science.1156965.
15. C. Lee, X. Wei, J.W. Kysar, J. Hone, Science. 321 (2008) 385–388. https://doi.org/10.1126/science.1157996.
16. A.A. Balandin, S. Ghosh, W. Bao, I. Calizo, D. Teweldebrhan, F. Miao, C.N. Lau, Nano Lett. 8 (2008) 902–907. https://doi.org/10.1021/nl0731872.
17. C. Vallés, C. Drummond, H. Saadaoui, C.A. Furtado, M. He, O. Roubeau, L. Ortolani, M. Monthioux, A. Pénicaud, J. Am. Chem. Soc. 130 (2008) 15802–15804. https://doi.org/10.1021/ja808001a.
18. D. Li, M.B. Müller, S. Gilje, R.B. Kaner, G.G. Wallace, Nat. Nanotechnol. 3 (2008) 101–105. https://doi.org/10.1038/nnano.2007.451.
19. X. Zhou, X. Huang, X. Qi, S. Wu, C. Xue, F.Y.C. Boey, Q. Yan, P. Chen, H. Zhang, J. Phys. Chem. C. 113 (2009) 10842–10846. https://doi.org/10.1021/jp903821n.
20. H. Li, X. Gui, L. Zhang, S. Wang, C. Ji, J. Wei, K. Wang, H. Zhu, D. Wu, A. Cao, Chem. Commun. 46 (2010) 7966–7968. https://doi.org/10.1039/C0CC03290E.
21. B. Li, H. Cao, J. Mater. Chem. 21 (2011) 3346–3349. https://doi.org/10.1039/C0JM03253K.
22. A.Y. Romanchuk, A.S. Slesarev, S.N. Kalmykov, D.V. Kosynkin, J.M. Tour, Phys. Chem. Chem. Phys. 15 (2013) 2321–2327. https://doi.org/10.1039/C2CP44593J.
23. X. Wang, L. Song, H. Yang, W. Xing, H. Lu, Y. Hu, J. Mater. Chem. 22 (2012) 3426–3431. https://doi.org/10.1039/C2JM15637G.
24. J. Ding, B. Li, Y. Liu, X. Yan, S. Zeng, X. Zhang, L. Hou, Q. Cai, J. Zhang, J. Mater. Chem. A. 3 (2014) 832–839. https://doi.org/10.1039/C4TA04297B.
25. C. Nethravathi, B. Viswanath, C. Shivakumara, N. Mahadevaiah, M. Rajamathi, Carbon. 46 (2008) 1773–1781. https://doi.org/10.1016/j.carbon.2008.07.037.
26. W. Katinonkul, M.M. Lerner, Carbon. 45 (2007) 2672–2677. https://doi.org/10.1016/j.carbon.2007.07.020.
27. N.A. Travlou, G.Z. Kyzas, N.K. Lazaridis, E.A. Deliyanni, Langmuir. 29 (2013) 1657–1668. https://doi.org/10.1021/la304696y.
28. G. Chen, M. Sun, Q. Wei, Y. Zhang, B. Zhu, B. Du, , J. Hazard. Mater. 244–245 (2013) 86–93. https://doi.org/10.1016/j.jhazmat.2012.11.032.
29. N. Baig, Ihsanullah, M. Sajid, T.A. Saleh, J. Environ. Manage. 244 (2019) 370–382. https://doi.org/10.1016/j.jenvman.2019.05.047.
30. K. Thakur, B. Kandasubramanian, J. Chem. Eng. Data. 64 (2019) 833–867. https://doi.org/10.1021/acs.jced.8b01057.
31. I. Ali, A.A. Basheer, X.Y. Mbianda, A. Burakov, E. Galunin, I. Burakova, E. Mkrtchyan, A. Tkachev, V. Grachev, , Environ. Int. 127 (2019) 160–180. https://doi.org/10.1016/j.envint.2019.03.029.
32. L. Liu, Y. Wan, Y. Xie, R. Zhai, B. Zhang, J. Liu, Chem. Eng. J. 187 (2012) 210–216. https://doi.org/10.1016/j.cej.2012.01.136.
33. L. Guimarães, A.N. Enyashin, G. Seifert, H.A. Duarte, Structural, J. Phys. Chem. C. 114 (2010) 11358–11363. https://doi.org/10.1021/jp100902e.
34. V. Vergaro, E. Abdullayev, Y.M. Lvov, A. Zeitoun, R. Cingolani, R. Rinaldi, S. Leporatti Biomacromolecules. 11 (2010) 820–826. https://doi.org/10.1021/bm9014446.
35. J. Xiao, X. Shaolei, Y. Jing, Y. Yao, X. Wang, Y. Jia, J. Mol. Liq. 220 (2016). 304-310. https://doi.org/10.1016/j.molliq.2016.04.057
36. J. Zare Pirhaji, F. Moeinpour, A. Mirhoseini Dehabadi, S.A. Yasini Ardakani, J. Mol. Liq. 300 (2020) 112345. https://doi.org/10.1016/j.molliq.2019.112345.
37. W.S. Hummers, R.E. Offeman, J. Am. Chem. Soc. 80 (1958) 1339–1339. https://doi.org/10.1021/ja01539a017.
38. Y. Yang, Y. Chun, G. Sheng, M. Huang, Langmuir. 20 (2004) 6736–6741. https://doi.org/10.1021/la049363t.
39. J. Duan, R. Liu, T. Chen, B. Zhang, J. Liu, Desalination. 293 (2012) 46–52. https://doi.org/10.1016/j.desal.2012.02.022.
40. G. Mishra, M. Mukhopadhyay, Sci. Rep. 9 (2019) 4345. https://doi.org/10.1038/s41598-019-40775-4.
41. Y. Liu, X. Jiang, B. Li, X. Zhang, T. Liu, X. Yan, J. Ding, Q. Cai, J. Zhang, J. Mater. Chem. A. 2 (2014) 4264–4269. https://doi.org/10.1039/C3TA14594H.
42. M.A. Ahmad, N.A. Ahmad Puad, O.S. Bello, Water Resour. Ind. 6 (2014) 18–35. https://doi.org/10.1016/j.wri.2014.06.002.
43. F. Çiçek, D. Özer, A. Özer, A. Özer, J. Hazard. Mater. 146 (2007) 408–416. https://doi.org/10.1016/j.jhazmat.2006.12.037.
44. D.K. Mahmoud, M.A.M. Salleh, W.A.W.A. Karim, A. Idris, Z.Z. Abidin, Chem. Eng. J. 181–182 (2012) 449–457. https://doi.org/10.1016/j.cej.2011.11.116.
45. A. Geethakarthi, B.R. Phanikumar, Kinetic and equilibrium studies, (2011).
46. B.A. Fil, C. Ozmetn, J. Chem. Soc. Pak. 34 (2012) 896–906.
47. C.K. Lee, K.S. Low, S.W. Chow, Environ. Technol. 17 (1996) 1023–1028. https://doi.org/10.1080/09593331708616471.
48. S. Netpradit, P. Thiravetyan, S. Towprayoon, J. Colloid Interface Sci. 270 (2004) 255–261. https://doi.org/10.1016/j.jcis.2003.08.073.

https://doi.org/10.51316/jca.2022.040